plate (thickness 1.6mm) (Fig.4). In this paper, monotonic tensile pilot tests were conducted to investigate the mechanical behavior of ductile knee brace members made of thin steel plates (hereafter referred to as the shear-yielding seismic dumper). The paper's purpose is to verify validity of stiffness and stress evaluation methods obtained in previous studies using the ordinary H section steel member, and to determine the stability of a load-deformation behavior of the shear-yielding seismic damper made of a thin steel plate.

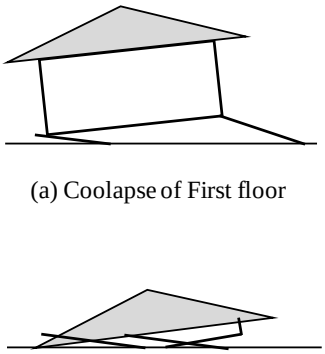

(a) Coolapse of First floor

(b) Coolapse of full floor

Fig. 1 – Collapse patterns of the wooden frame

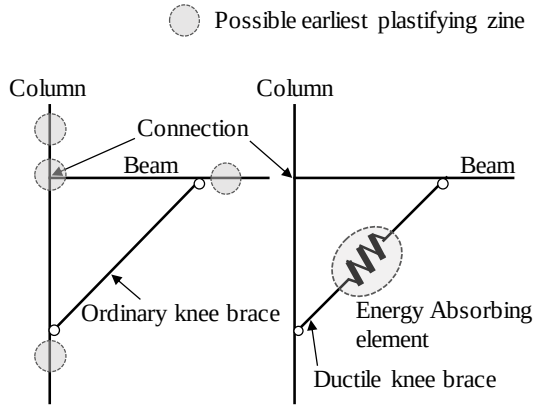

(a) Ordinary knee brace (b) Ductile knee brace

Fig. 2 – Reinforcement by the knee braces

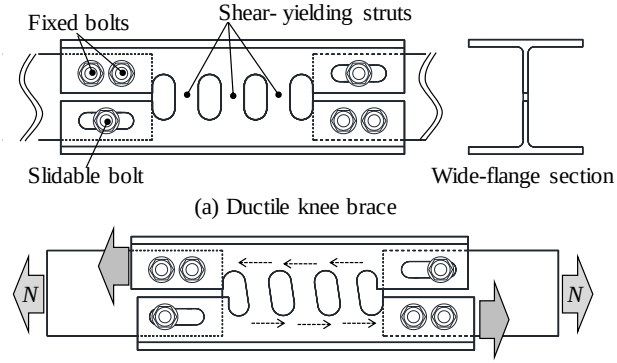

Fig. 3 – Concept of the ductile knee brace

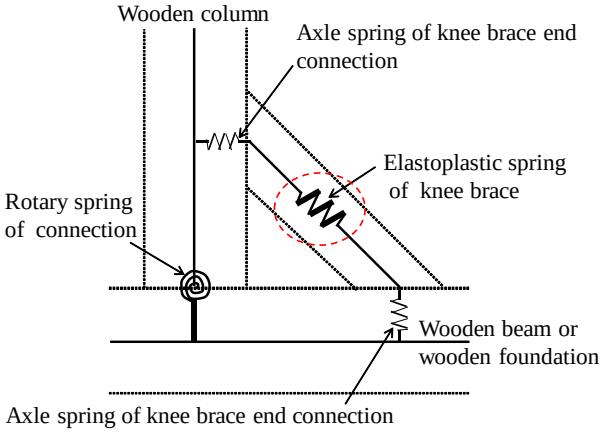

Fig. 4 – Application of the ductile knee brace to the wooden frame

2. Experimental plan

2.1 Outline of specimens

Fig. 5 depicts outlines of the test specimens. The specimen is made of a thin steel plate (140 × 300 × 1.6mm) manufactured by bending the plate inward by 20mm from both sides so that it becomes C shaped. The strut in the web is shaped like (a) a rectangle or (b) a pounder (Fig.6). Mechanical properties of the steel material are summarized in Table 1. The end of the knee brace is connected to gusset plates via three high-strength bolts with standard and slotted holes. Four bolts with standard holes are for slip-critical connections and two other bolts with slotted holes are snug-tightened so that they can slide.

Table 2 presents a list of test specimens. There are four test specimens: two rectangular and two pounder shaped—made of different taper angles. The structure performance of the shear-yielding seismic damper mainly depends on the following parameters: number of struts n_{st}, height of the strut h_{cb}, thickness of the web t_w, width of the strut w_{st}, center width of the strut b_{cb}, radius of the strut end r_{sl}, and yield stress of the thin steel plate. The test parameters are the number of struts (n_{st}) in a uniform section, radius of the strut end r_{sl}, and yield stress of the thin steel plate in a variable section; the specimen is expressed as Cn_{st}-h_{cb}-r_{sl}.

2.2 Methods of a loading and measuring deformations

The loading is displacement-controlled by the overall deformation of the shear-yielding seismic damper. The monotonic tensile loading test is continued until the bolt set at the center of the slotted hole reaches the inside of the hole-edge.

The positions of the displacement transducer are depicted in Fig.7, and an overall deformation of the shear-yielding seismic damper and local deformation of a strut in the damper are measured by two displacement transducers. The overall deformation δ_a is measured by the distance (300mm) between both outsides of the specimen. On the other hand, local deformation of the strut δ_l is measured by the distance (50mm) between near the upper and lower ends of the strut as the relative displacement between them.

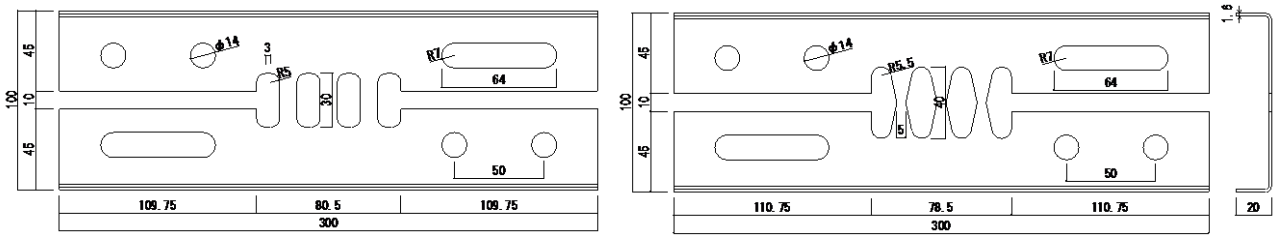

(a) Example of a rectangular shape (C3-30-5) (b) Example of a pounder shape (C3-40-5.5)

Fig. 5 – Test specimens

Table 1 – Mechanical properties of steel materials

Specimen type	t_{st} (mm)	Yield stress (N/mm^2)	Tensile stress (N/mm^2)	Yiled ratio (%)	Young's modulus ($\times 10^5$N/mm^2)
SS400	1.6 (1.51)	272	384	80	1.80

Table 2 – Parameters in the strut

Specimen	t_w mm	n_{st}	h_{cb} mm	r_{sl} mm	w_{st} mm	b_{cb} mm
C2-30-5	1.6	2	30	5	9.5	-
C3-30-5		3	30	5	9.5	-
C3-40-4		3	40	4	16.5	5
C3-40-5.5		3	40	5.5	13.6	5

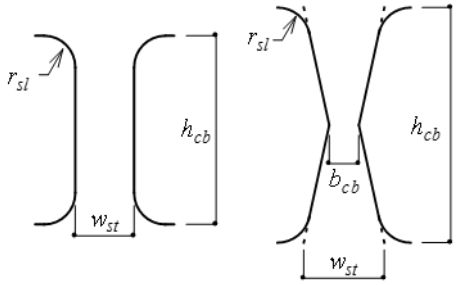

(a) Rectangular shape (b) Pounder shape

Fig. 6 – Strut dimensions

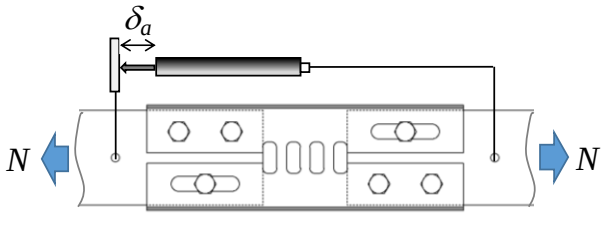

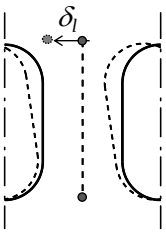

(a) Overall deformation (b) Local drift deformation of the strut

Fig. 7 – Positions of the displacement transducer

3. Test Results

3.1 N-δ_a and δ_l relationship curves

Figs. 8 (a)–(d) show the experimental N-δ_a and N-δ_l relationship curves for all specimens, respectively, and experimental yield strength ${}_{exp}N_y$, full plastic strength ${}_{exp}N_p$, estimated yield strength ${}_{cal}N_y$, and full plastic strength ${}_{cal}N_p$ are shown in the same figure. Each initial stiffness is shown as a ${}_{exp}k_a$ and ${}_{exp}k_l$ in the N- δ_a and δ_l relationship curves, respectively. The experimental yield strength ${}_{exp}N_y$ and full plastic strength ${}_{exp}N_p$ are decided by the general yield point method as follows:

The experimental full plastic strength ${}_{exp}N_p$ is the load corresponding to the intersection of the initial stiffness line and tangent line at a point on the load-deformation curve corresponding to 1/2 of the deformation δ_T, and the experimental yield strength ${}_{exp}N_y$ is the load corresponding to the intersection of the load-deformation curve and the perpendicular drawn down from the intersection of the initial stiffness line and tangent line (Fig. 9). On the other hand, the estimated yield strength ${}_{cal}N_y$ and full plastic strength ${}_{cal}N_p$ are calculated by the evaluation formula proposed in previous papers [1] and [2]. Table 3 shows the initial stiffness ${}_{exp}k_a$, second stiffness ${}_{exp}k_2$, and third stiffness ${}_{exp}k_3$ in the N-δ_a relationship curves, and initial stiffness of the local deformation ${}_{exp}k_l$ in the N-δ_l relationship curves.

3.2 Specimens after loading testes

In the final loading step, it was confirmed that struts in the test specimen were twisted out of plane (Fig.9). This was not seen in previous experiments using ordinary steel members, and is detailed in the next section.

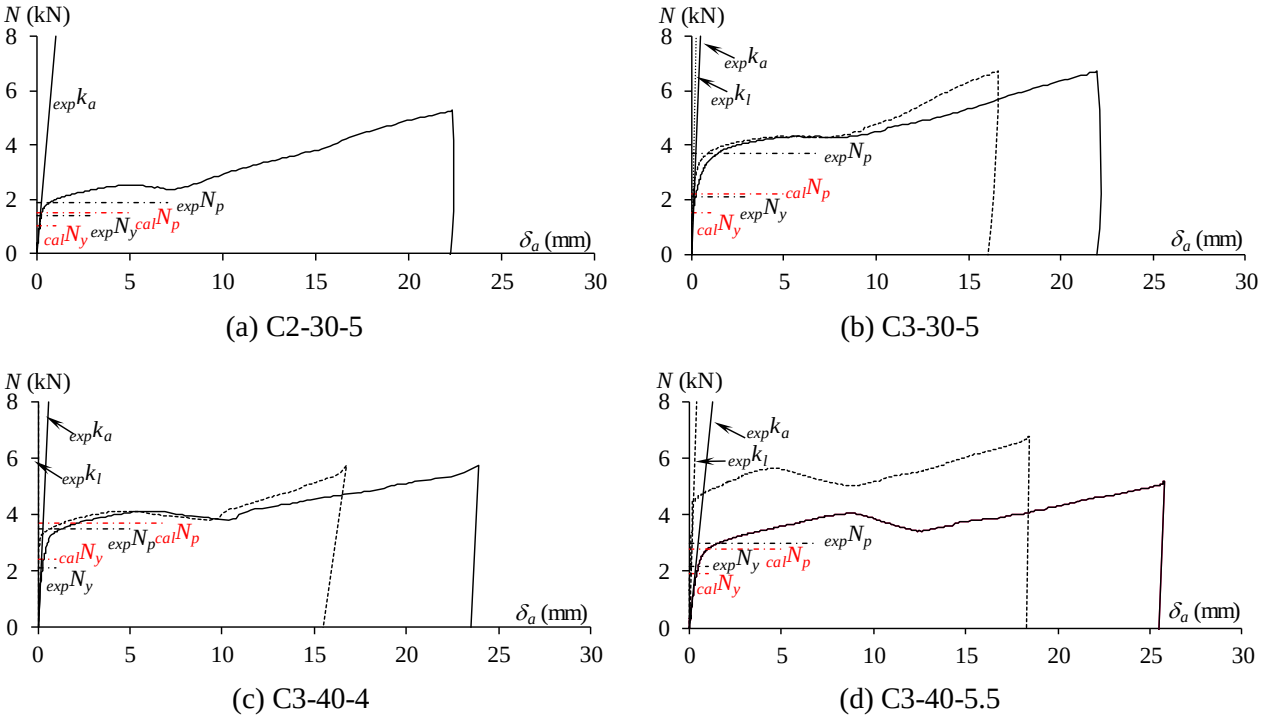

(a) C2-30-5 (b) C3-30-5

(c) C3-40-4 (d) C3-40-5.5

Fig. 8 – Axial force input to the knee brace N- Overall deformation δ_a

Table 3 – Experimental initial rigidity and comparison of yield strength and full plastic strength

Specimen	$_{exp}k_a$ (kN/mm)	$_{exp}k_l$ (kN/mm)	$_{exp}N_y$ (kN)	$_{exp}N_p$ (kN)	$_{cal}N_y$ (kN)	$_{cal}N_p$ (kN)
C2-30-5	7.90	-	1.43	1.95	1.02	1.48
C3-30-5	16.20	36.15	1.70	3.68	1.53	2.22
C3-40-4	14.17	173.83	2.10	3.46	2.49	3.74
C3-40-5.5	6.27	20.20	2.18	3.05	1.88	2.81

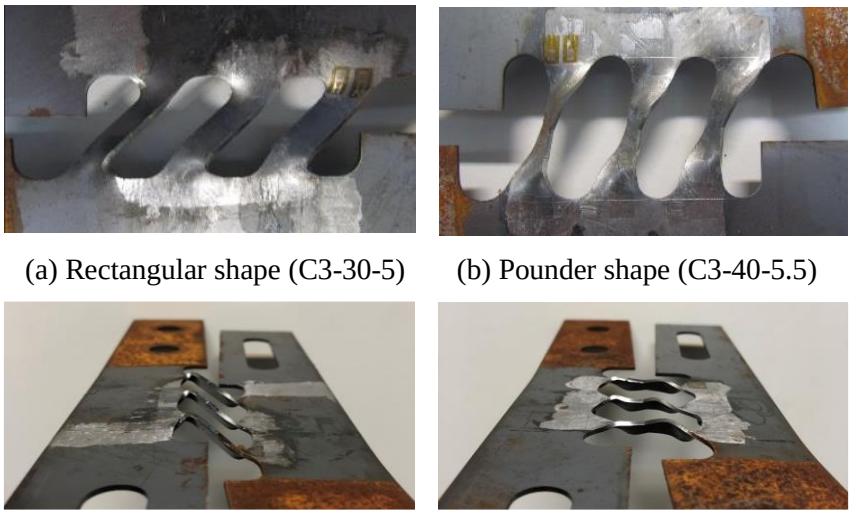

(a) Rectangular shape (C3-30-5) (b) Pounder shape (C3-40-5.5)

(c) Tortional buckling (C3-30-5) (d) Tortional buckling (C3-40-5.5)

Fig. 9 – Photo of the specimen after loading test

4. Discussion of the load-deformation behavior

4.1 Transition of the load-deformation behavior

Fig. 10 shows a transition of the relationship between the tensile load and the overall deformation of the shear-yielding seismic damper made of a thin steel plate. Changes in the condition of the specimen during loading were generally as follows: (I) The strut was not deformed out-of-plane by the shear force even when the yield strength ($_{exp}N_y$) and the full plastic strength ($_{exp}N_p$) were exhibited, but the strut was deformed in-plane by the shear force. (II) After reaching the full plastic strength ($_{exp}N_p$), no out-of-plane deformation was observed, and strength continued to increase. (III) However, out-of-plane twisting was caused by upper and lower ends of the strut, and when such behavior was observed, the load began to decrease almost at the same time, and the load decreased slightly until a lateral torsional buckling became clear. (IV) Further, after the lateral torsional buckling became clear, the load increased again.

The maximum strength $_{exp}N_T$ and minimum strength $_{exp}N_L$ immediately after the full plastic strength are presented in Fig.9, respectively. Moreover, the strength at the finish of the loading is defined as $_{exp}N_u$ (Fig.10), and their values ($_{exp}N_T$, $_{exp}N_L$, $_{exp}N_u$) and $_{exp}N_y$, $_{exp}N_p$ are presented in Table 4. The deformation values corresponding to their strengths are presented in Table 5.

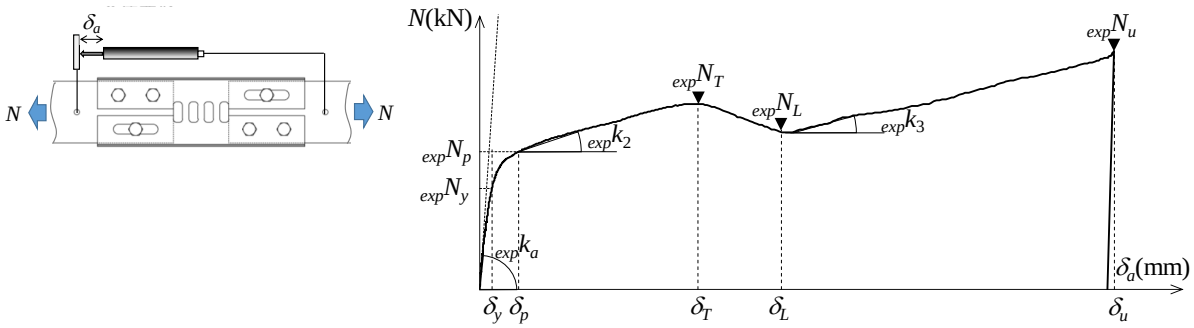

Fig. 10 – Transition of the tensile load N- Overall deformation δ_a relationship curves

Table 4 – Various strengths in transition of the load-deformation behavior

Specimen	$_{exp}N_y$ (kN)	$_{exp}N_p$ (kN)	$_{exp}N_T$ (kN)	$_{exp}N_L$ (kN)	$_{exp}N_u$ (kN)
C2-30-5	1.43	1.95	2.52	2.37	5.30
C3-30-5	1.70	3.68	4.33	4.32	6.74
C3-40-4	2.10	3.46	4.12	3.82	5.76
C3-40-5.5	2.18	3.05	4.05	3.47	5.19

Table 5 – Various deformations in transition of the load-deformation behavior

Specimen	δ_y (mm)	δ_p (mm)	δ_T (mm)	δ_L (mm)	δ_u (mm)
C2-30-5	0.25	0.89	4.75	7.13	22.34
C3-30-5	0.22	1.36	5.45	6.09	21.99
C3-40-4	0.24	1.29	6.32	10.38	23.92
C3-40-5.5	0.49	1.75	8.72	12.07	25.76

4.2 Plastic deformation ratio

Figure 11 presents nondimensional results obtained by dividing a load axis of the load-deformation relationship by full plastic strength, and a deformation axis of the load-deformation relationship by the elastic deformation corresponding to the full plastic strength ($_{exp}N_p$ / $_{exp}k_a$). The plastic deformation ratio corresponding to various strengths is presented in Table 6. Since the horizontal axis in Figure 11 is the amount equivalent to the plastic deformation ratio, the value of the horizontal axis at various strengths are represented as μ_T, μ_L, and μ_u. Immediately before the beginning point of the lateral torsional buckling μ_T is a value from 18 to 25, and the difference between specimens are relatively small. On the other hand, when the morphology of the lateral torsional buckling is stable, the value μ_L is a value between 25 and 43. Furthermore, the difference between test specimens is slightly large. μ_u at the finish of the experiment is the value from 91 to 100 except for specimen C3-40-5.5, and the value is almost identical (Table 6).

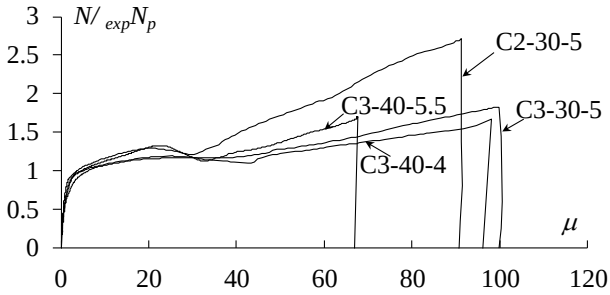

Fig. 11 – Non-dimensional load-deformation relationship

Table 6 – Plastic deformation ratio

Specimen	μ_T	μ_L	μ_u
C2-30-5	19	29	91
C3-30-5	25	28	100
C3-40-4	25	43	98
C3-40-5.5	18	25	53

4.3 Rigidity

Table 7 shows the ratio of the initial stiffness $_{exp}k_a$ (= 1) to the second stiffness k_2 in the nondimensional load-deformation relationship, and the ratio of the third stiffness to the initial stiffness $_{exp}k_a$ (= 1) in the nondimensional load-deformation relationship (after strength decreases, the ratio of the stiffness that rises again) k_3. Table 4 indicates that k_2 and k_3 of specimens C2-30-5 and C3-40-5.5 are the value from 1.95 / 100 to 2.47 / 100 times the initial stiffness. Since the rigidity ratio of C3-30-5 and C3-40-4 is the value from 0.80 / 100 to 1.13 / 100 times, the graph in Fig.3 is divided into two groups based on characteristics of the rigidity ratio. Within this experiment, the rigidity k_2 and k_3 of both groups are almost identical.

4.4 Evaluating lateral torsional buckling

Reference [5] describes the evaluation strength of hysteretic steel dampers with butterfly-shaped links in three limit states (flexural yielding, shear yielding, and elastic lateral torsional buckling), and the butterfly-shaped damper is similar to the shear-yielding seismic damper in this paper. Moreover, [5] proposes an evaluating equation for the elastic lateral torsional buckling per strut.

$$V_{cr} = \frac{2Ebt^3}{L^2\sqrt{1+v}}[0.096(a/b)^3 - 0.281(a/b)^2 + 0.547(a/b) + 0.533] \quad (1)$$

Here, V_{cr}: shear force associated with elastic lateral torsional buckling, E: Young's modulus, b: width of strut upper and lower ends, a: central width of the strut, t: plate thickness, L: height of the strut, v: Poisson's ratio (= 0.3). $a = b$ in the rectangular-shaped specimen in this study. Table 8 shows parameters and the shear force associated with elastic lateral torsional buckling.

The shear force associated with elastic lateral torsional buckling V_{cr} are much larger than ${}_{exp}N_T$ and ${}_{exp}N_L$ in this experiment. The lateral torsional buckling phenomenon in this experiment cannot be evaluated as an elastic problem.

Table 7 – Second and third stiffness in the nondimensional relationship

Specimen	k_2 (1.0×10^{-2})	k_3 (1.0×10^{-2})
C2-30-5	1.97	2.47
C3-30-5	1.00	1.13
C3-40-4	1.09	0.80
C3-40-5.5	2.19	1.95

Table 8 – Lateral torsional buckling strength and Parameters

Specimen	L (mm)	a (mm)	b (mm)	V_{cr} (kN)
C2-30-5	30	9.5		20.54
C3-30-5	30	9.5		30.81
C3-40-4	40	5	16.5	20.46
C3-40-5.5	40	5	13.6	17.01

5. Conclusions

The yield strength and full plastic strength of the knee brace members made of thin steel plates were investigated by a series of monotonic loading tests. The strengths can be evaluated by using previous evaluation formulas based on the specimens with thicker plates, although the strengths are slightly underestimated. However, considering the occurrence of the lateral torsional buckling as observed in these test specimens, it should be considered that there is an effective deformation range for the stable performance as the seismic damper. In these tests, the deformation range may correspond to about 20 in terms of the plastic deformation ratio. These results were obtained under monotonic loading tests, and cyclic loading tests have not been conducted yet; future studies must confirm a primary factor of lateral torsional buckling under cyclic loading.

6. Acknowledgements

This work was supported by JSPS KAKENHI Grant Numbers 19K15081. The authors are grateful to Mr. Eon Koshimori (AI SEKKEI Corporation) for his support in conducting tests of ductile knee braces made of thin steel plates.

7. Copyrights

8. References

[1] S. Honma, K. Ebato, and Y. Harada: Study on structural behavior of weldless joint in beam-to-column connection of interior column with knee brace, STESSA 2012, Santiago, Chile, 263-268, 2012. 1

[2] S. Honma, Y. Harada, and K. Ebato: Mechanical Behavior of Ductile Steel Knee-Brace whose Damping Portion has Non-Uniform Section, Summaries of technical papers of annual meeting of Architectural Institute of Japan, C-1 Structure Ⅲ, pp. 1111-1112, 2015 (in Japanese)

[3] Sayuri HONMA**,** Yukihiro HARADA, Kazumasa EBATO: Estimation Method on Hysteresis Characteristics of Subassemblage with Ductile Knee-Brace Member, 9th International Conference on Behavior of Steel Structures in Seismic Areas(STESSA2018) Christchurch, New Zealand, 2018. 2.

[4] Fuminobu OZAKI, Yoshimichi KAWAI, Ryoichi KANNO, Koji HANYA: Developments of damage-control systems for cold-fomed steel structures, Kou kouzou rombunshuu, Vol. 21, No. 82, 63-74, 2014. 3. (in Japanese)

[5] Alireza Farzampour, Matthew R. Eatherton: Yielding and lateral torsional buckling limit states for butterfly-shaped shear links, Engineering Structures, Vol. 180, 442–451, 2019.

